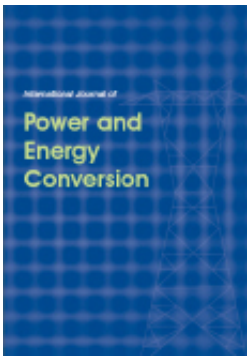

International Journal of Power and Energy Conversion

ISSN online: 1757-1162 - ISSN print: 1757-1154
https://www.inderscience.com/ijpec

Effect of pH on the physical properties of grown nickel oxide by SILAR experimental technique and numerical investigation as the hole transport layer for high energy conversion perovskite solar cell

Khalid Fathi, Yassine Salhi, Nabil Bouri, Mounir Fahoume, Mounia Tahri, Khalid Nouneh

DOI: 10.1504/IJPEC.2024.10062384

Article History:

Received:	28 August 2023
Last revised:	27 September 2023
Accepted:	28 September 2023
Published online:	22 February 2024

Effect of pH on the physical properties of grown nickel oxide by SILAR experimental technique and numerical investigation as the hole transport layer for high energy conversion perovskite solar cell

Khalid Fathi

Laboratory of Materials Physics and Subatomic,
Faculty of Sciences,
University Ibn Tofail,
BP 133, 14000,
Kenitra, Morocco
and
National Centre for Nuclear Energy, Science and Technology,
Rabat, Morocco
Email: fathi@cnesten.org.ma

Yassine Salhi, Nabil Bouri and Mounir Fahoume

Laboratory of Materials Physics and Subatomic,
Faculty of Sciences,
University Ibn Tofail,
BP 133, 14000,
Kenitra, Morocco
Email: yassine.salhi1@uit.ac.ma
Email: nabil.bouri@uit.ac.ma
Email: mounir.fahoume@uit.ac.ma

Mounia Tahri

National Centre for Nuclear Energy, Science and Technology,
Rabat, Morocco
Email: tahri@cnesten.org.ma

Khalid Nouneh*

Laboratory of Materials Physics and Subatomic,
Faculty of Sciences,
University Ibn Tofail,
BP 133, 14000,
Kenitra, Morocco
Email: khalid.nouneh@uit.ac.ma
*Corresponding author

Abstract: Nickel oxide thin films have been prepared using successive ionic layer adsorption and reaction method on soda lime glass substrate. In this work, we report the synthesis and the influence of the number of cycles (N = 20, 60 and 80 cycles) and pH = 12, pH = 14 on structural, morphological, and optical properties of the synthesised NiO thin films onto a glass substrate. The prepared films were characterised by X-ray diffraction spectroscopy (XRD), UV-Vis NIR spectroscopy, scanning electron microscopy (SEM) and energy dispersive analysis (EDS). The film elaborated at pH = 14 for 60 dipping cycles exhibits good morphology and crystallinity. It has a band gap of 3.44 eV and a transmittance of 86%. Optimisation and simulation from the SCAPS-1D simulator demonstrate that our NiO optimised film can be used as hole transport layer (HTL) for perovskite solar cells to yield a power conversion efficiency (PCE) of 18.11%.

Keywords: PH; silar; Raman; FTIR; scaps simulator; hole transport layer; HTL; power conversion efficiency; PCE; perovskite solar cell; PSC.

Reference to this paper should be made as follows: Fathi, K., Salhi, Y., Bouri, N., Fahoume, M., Tahri, M. and Nouneh, K. (2024) 'Effect of pH on the physical properties of grown nickel oxide by SILAR experimental technique and numerical investigation as the hole transport layer for high energy conversion perovskite solar cell', *Int. J. Power and Energy Conversion*, Vol. 15, No. 1, pp.57–78.

Biographical notes: Khalid Fathi is a PhD student at the Laboratory of Materials Physics and Subatomics (LMPS), Department of Physics, Faculty of Science, Ibn Tofail University (Kenitra, Morocco). He is also a senior manager and expert of microelectronics, renewable energy, and materials and he is responsible for maintenance in the Radioactive Waste Management Unit (UGDR) at the National Centre for Nuclear Energy, Sciences and Technology (CNESTEN), Morocco.

Yassine Salhi has obtained his PhD in Fundamental and Applied Chemistry from the Ibn Tofail University, Morocco in 2019. He is a researcher at the Laboratory of Organic Chemistry, Catalysis and Environment, Department of Chemistry, Faculty of Science, Ibn Tofail University since July 2019. He is also a researcher with Materials, Nanomaterials and Applications (MANA) Team at the Laboratory of Materials Physics and Subatomic, Faculty of Science, Ibn Tofail University since September 2021. He is an experienced researcher in electrochemistry and nanomaterials for solar cells applications.

Nabil Bouri is a PhD student at the Laboratory of Materials Physics and Subatomics (LMPS), Department of Physics, Faculty of Science, Ibn Tofail University (Kenitra, Morocco). He is an expert in the simulation of solar cells and applications.

Mounir Fahoume is a Professor (full). He is an expert in thin films and nanostructures for solar cell applications.

Mounia Tahri is currently scientist researcher (PhD in Physical Analysis and Environment) and the Head of Geochemistry and Chemical Pollution in National Centre for Nuclear Energy, Sciences and Technology in Morocco. She has valuable experience in the field of XRD analysis and environment monitoring and has more than 70 refereed publications.

Khalid Nouneh is an Associate Professor and the Head of MANA Team at the Department of Physics, Ibn Tofail University, Morocco. He is an expert in thin films and nanostructures for energy and environment.

1 Introduction

Metal oxides are promising materials for solar cell (SC) applications. Among them, we find nickel oxide NiO thin film which has attracted the attention of researchers to develop advanced materials for a wide range of applications in the photovoltaic domain. The use of such metal oxide is not limited to SCs, but other applications are also targeted. Since NiO thin films possess original electrical and optical properties, they are widely used in a variety of applications, including electrochromic coatings, anti-ferromagnetic materials, transparent electrodes, electrochemical capacitors, photocatalysis, chemical sensors, lithium-ion batteries, and dye-sensitised SCs (Dridi et al., 2023).

NiO thin film is a transparent conductive oxide (TCO). It is a p-type oxide semiconductor with an energy band gap between 3.6 and 4.0 eV (Dridi et al., 2023; Aivalioti et al., 2023; Kaya et al., 2021). Several types of heterojunctions have been formed combining p-NiO with n-type semiconductors such as Si, GaN, InN, Ga_2O_3, ZnO, ITO or TiO_2 and even p/n NiO homojunction (Aivalioti et al., 2023).

Enhancing SC efficiency requires the use of advanced materials to achieve this goal. NiO is one of the promising materials to do so. This metal oxide finds its application in perovskite and halide perovskite solar cells (PSCs) as hole transport layer (HTL) (Mattaparthi et al., 2023; Qin et al., 2019; Cai et al., 2023) silicon SCs as an antireflection layer (Jlassi et al., 2017), GeSe thin film-based SC as back surface field layer (Zhao et al., 2022), CIGS thin-film SCs as functional-window thin layer (Youn et al., 2020) and last but not least in CdTe thin film SC as a back contact buffer layer (Xiao et al., 2017). Several techniques can be used to prepare NiO thin films, including sputtering (Srivastava et al., 2023; Tang et al., 2023; Terlemezoglu et al., 2022; Şenaslan et al., 2021; Usha et al., 2022), sol-gel (Jlassi et al., 2017; Aswathy et al., 2020, 2022), spray pyrolysis (Owoeye et al., 2023; Aftab et al., 2021; Obaida et al., 2022; Ganesh et al., 2021; Javadian and Fadavieslam, 2022; Ade et al., 2022), spin coating (Vijaya Prasath et al., 2022; Chtouki et al., 2021), electrodeposition (Quispe et al., 2021; Bahramian et al., 2019; Bulakhe and Deokate, 2022; Hosseinzade et al., 2022), solvothermal synthesis (Gutierrez et al., 2013), hydrothermal synthesis (Goel et al., 2022), pulsed laser deposition (Ai et al., 2008; Fasaki et al., 2010), electron-beam evaporation (Ganga Reddy et al., 2002; Jiang et al., 2012) and SILAR (Nachammai et al., 2022; Das et al., 2018; Taşdemirci, 2019; Klochko et al., 2018; Akaltun and Çayır, 2015).

The present work focuses on SILAR technique as one of the low-cost techniques to fabricate nickel oxide thin films. Even though SILAR technique is a cheap and practical way to obtain NiO thin films, only a few studies have employed it to develop this metal oxide. The purpose of this paper is to present the SILAR technique and outline its benefits for producing NiO thin films for SC applications.

Thus, the advantages of SILAR method are (Woo-García et al., 2022; Calixto-Rodriguez et al., 2021; Sundhar, 2022; Soonmin, 2022):

- Large area deposition on any substrate at lower temperatures (room temperature) with simple techniques and low-cost instruments (simple dip coating unit).
- Control of stoichiometry, thickness, morphology, and grain size of the material (via solution concentration and number of cycles up to micrometers).
- No vacuum chamber required (mostly close to room pressure).

- Excellent growth rate with no precipitate.

2 Experimental

In this study, NiO films were prepared by using SILAR process. Nickel chloride hexahydrate ($NiCl_2.6H_2O$) was used as a cationic precursor and it was dissolved in de-ionised water. The concentration value of nickel chloride was fixed to 0.1 M to be able to study the impact of other parameters such as: annealed, un-annealed, pH and temperature according to Table 1. The pH value was adjusted to 12 and 14 by adding aqueous Ammonia NH_3. During the film deposition the distilled water was maintained at a temperature of 85°C and the precursor solution was kept at room temperature. Adsorption, reaction and rinsing times were set constant for these films. One SILAR cycle contained four steps:

1 the substrate was first immersed in precursor solution

2 rinsed in distilled water

3 immersed in alkaline solution

4 rinsed in distilled water.

Table 1 Samples description of 2 h annealed NiO thin films at 550°C deposited by SILAR technique

Samples	a	b	c	d	e	f
pH	12	12	12	14	14	14
Cycles	20	60	80	20	60	80

The immersion time of the substrate for one cycle in each solution was for 30 seconds. By repeating such continuous deposition cycles (20–60 and 80) according to each sample a thin film of NiO was formed on the glass substrate in different range thicknesses. The reaction of NiO thin film formation can be written as:

First nickel chloride will dissociate in water to give nickel cations according to the following reaction:

$$NiCl_2 \cdot 6H_2O \rightarrow Ni^{2+}(aq) + 2Cl^{-}(aq) \quad (1)$$

Then ammonia will dissociate in water to give ammonium ion and hydroxide ion

$$NH_3 + H_2O \rightarrow NH_{4+} + OH^{-} \quad (2)$$

After that nickel cations will form NiO with hydroxide ions:

$$Ni^{2+} + 2OH^{-} \rightarrow NiO + H_2O \quad (3)$$

After that, the grown NiO samples were annealed at 550°C for 2 h.

3 Results and discussion

3.1 XRD analysis

X-ray diffraction spectroscopy (XRD) analysis has shown that the NiO thin film deposited for 60 dipping cycles with 550°C annealing (sample e) displayed the best crystallinity among the deposited NiO thin films of this study. Furthermore, the three characteristic peaks at 36,46°, 42,56° and 62,16° in this NiO thin film have only been identified as peaks of cubic NiO crystallites along the diffraction planes (111), (200) and (220) with respect to the (JCPDS Card 47-1049) as shown in Figure 1.

The crystallite size of the NiO thin film was calculated from the FWHM of the diffraction plane using Debye Scherrer's formula:

$$D = \frac{\lambda K}{\beta \cos\theta}$$

The value of dislocation density (d) is using the relation,

$$\Delta = \frac{1}{D^2}$$

The d-spacing is calculated using the relation,

$$d = \frac{n\lambda}{2\sin\theta}$$

Figure 1 XRD pattern of NiO thin films (sample e) grown at pH = 14 for 60 dipping cycles and annealed at 550°C for 2 h (see online version for colours)

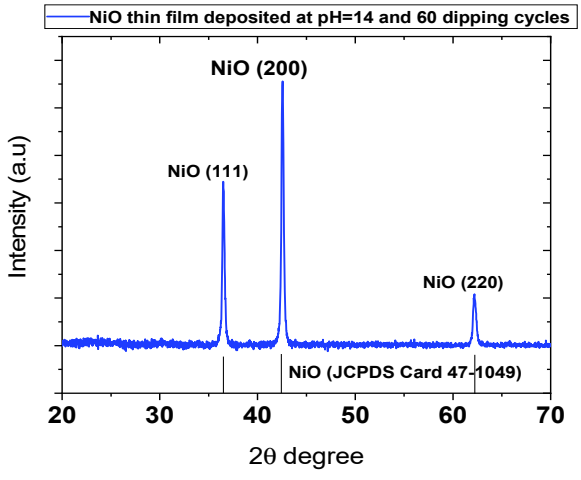

The XRD parameters of the NiO thin film grown at pH = 14 for 60 dipping cycles and annealed at 550°C are tabulated in Table 2.

Table 2 XRD parameters calculations for NiO thin films grown at pH = 14 for 60 dipping cycles and annealed at 550°C

Crystallite size D (nm)	*Dislocation density ($\delta \times 10^{15}$ l/m)*	*d-spacing (A°)*
29	1.2	2.45

3.2 SEM and EDX analysis

Figure 2 displays scanning electron microscopy (SEM) images of the as-prepared samples a, b, c, d, e and f. The elaborated NiO thin film at pH = 14 for 60 dipping cycles (sample e) has the better surface morphology with total and porosity which confirms the XRD analysis. For pH = 12, the NiO thin films have bad surface morphology with cracks in the case of 60 and 80 dipping cycles (samples b and c) due to bad thin film quality as grown and annealed. Although, the SEM images of NiO thin film deposited at pH = 14 have improved surface morphology, but the one with 60 dipping cycles remains the one with the best surface morphology. The film is adherent, homogenous, and porous due to the pH = 14 and the 40 dipping cycles. It consists of nearly the 1:1 stoichiometry since both atomic ratios are nearly the same (50%) as shown in Figure 2. Figure 2(e) shows the morphological image of the elaborated NiO thin film at pH = 14 for 60 dipping cycles. From the figure, well adherent and porous, thin film has been formed due to increasing alkalinity (pH = 14) and increased number of cycles which has increased the nucleation growth rate so as to form thin film by adsorption (Nachammai et al., 2022). Consequently, this yields well sized particles and good coverage in the case of pH = 14 in comparison with thin films elaborated at pH = 12 regardless of the number of dipping cycles. Cracks in the case of pH=12 for 60 and 80 dipping cycles can be seen in the SEM images [Figures 2(b) and 2(c)]. This might explain the deterioration in the films due to the decrease in nucleation growth rate at pH = 12 which gives films that are poorly coated and undergo cracks after annealing as results. The porosity in the case of the NiO thin film grown at pH = 14 and for 60 dipping cycles is due to the releasing of strain energy and removal of defect (Das et al., 2018). Thus, after annealing, the thin film is free of cracks. Increasing the pH from 12 to 14 has significantly improved both surface morphology and crystallinity of the thin film. In addition to this, increasing dipping cycles from 20 to 60 in the case of the pH = 14 has noticeably improved the thin film quality both on structural and morphological levels but at 80 cycles, the quality of the film was relatively bad. In this case, the thin film quality directly depends on the pH value. The formed particles were highly agglomerated and well crystallised after annealing. Figure 3 shows the EDX spectrum of the annealed NiO thin film for 60 dipping cycles at pH = 14. From the figure it was confirmed that the presence of Ni and O elements in the NiO thin film.

As a result, increasing the pH value from 12 to 14 has remarkably improved the surface morphology and the crystallinity of NiO thin film especially at 60 dipping cycles but going beyond this will strongly affect the thin film quality in term of crystallinity and morphology. The optical study will confirm the XRD and SEM characterisation. The NiO thin film elaborated at pH = 14 and for 60 dipping cycles should meet the requirement of an HTL layer for a PSC in term of band gap energy and transmittance which must be higher for better power conversion efficiency (PCE) of the PSC.

Figure 2 SEM images of NiO thin films: pH = 12: (a) 20 cycles (b) 60 cycles (c) 80 cycles and pH = 14: (d) 20 cycles (e) 60 cycles (f) 80 cycles

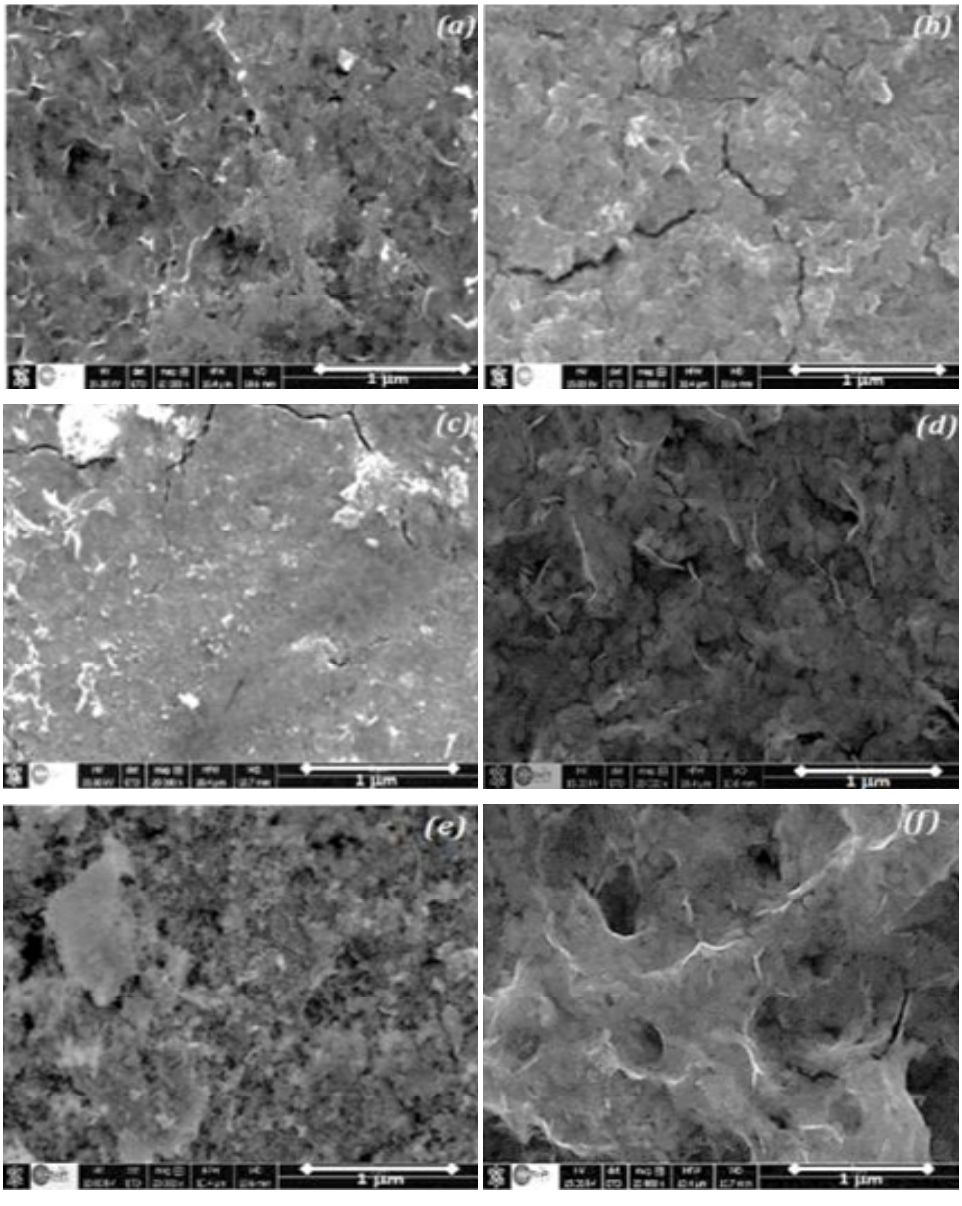

3.3 Optical characterisation

It has been demonstrated that the pH = 14 is the suitable value to grow NiO thin films with good quality. So, the optical study will focus on the thin films grown at pH = 14 for 20, 60 and 80 cycles. The optical study must confirm the SEM and XRD analysis. Apparently, the NiO thin film grown at pH = 14 for 60 cycles must be the one with the higher transmittance since it was adherent, and homogenous with good surface

morphology, but the optical characterisation is the key to using an appropriate HTL layer for a PSC for the highest PCE which is very crucial in manufacturing and commercialising a SC. The optical transmittances for the NiO films are shown in Figure 4. The films exhibit transmittance ranging from 56% to 86% in the visible to near-infrared region. From the graph it is observed that the dipping cycles were increased but the transmittance of the last film with 80 dipping cycles decreased with the increase in the number of dipping cycles. This is related to an overload of the film deposition which has affected its quality even with increased dipping cycles. So, the number of cycles is limited to 60 cycles to grow a film with good morphological, structural and as a result optical characteristic. As seen in Figure 5, the optical band gap (E_g) of the NiO films increased after increasing dipping cycles up to 60 cycles and decreased when the number of cycles reached 80 which is very normal as the transmittance of the last film decreases instead of increasing. Thus, the same is true for the band gap. The values of the band gap of each film are summarised in Table 3.

Figure 3 EDX analysis for NiO thin film (60 dipping cycles; pH = 14) (see online version for colours)

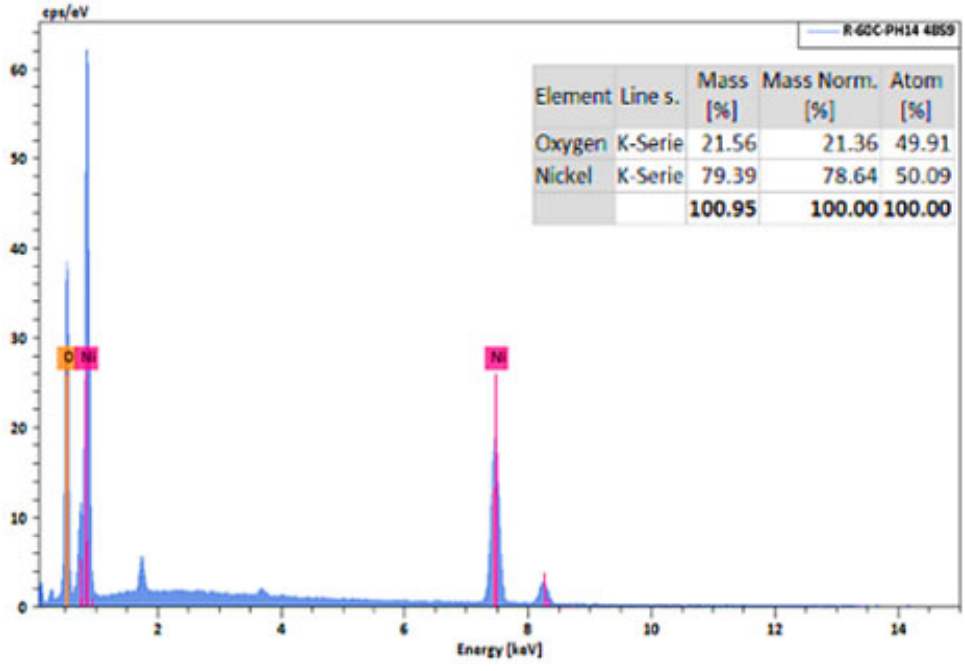

Table 3 Optical parameters of annealed and grown NiO films: pH = 14 for 20, 60 and 80 dipping cycles

Number of cycles	20	60	80
Transmittance (%)	78	86	50
Band-gap E_g (eV)	3.27	3.44	3.18

Figure 4 Transmittance spectra of NiO thin film elaborated at pH = 14 for 20, 60 and 8 dipping cycles (see online version for colours)

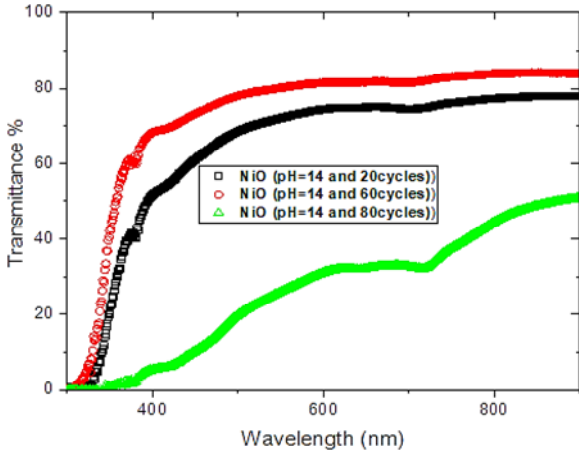

Figure 5 Band gap (E_g) spectra of NiO thin films elaborated at pH = 14 for, (a) 20 (b) 60 (c) 80 dipping cycles (see online version for colours)

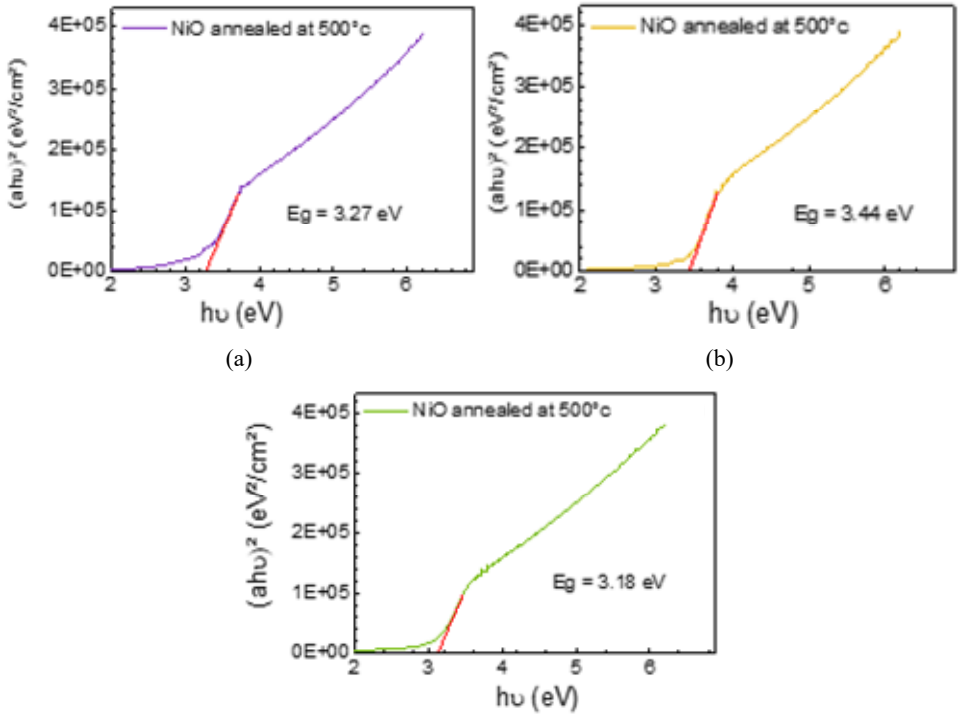

(a) (b)

(c)

3.4 Raman analysis

Based on the Raman spectra recorded from 450 cm^{-1} to 1,800 cm^{-1} ranges, the film synthesised on ITO displays spectra with principal peaks recorded at about 502 cm^{-1} (Qiu et al., 2023) 570 cm^{-1}, 906 cm^{-1} (Mironova-Ulmane et al., 2007), 1,078 cm^{-1} (Qiu et al., 2022), between 1,100 and 1,200 cm^{-1} (Feldl et al., 2020), between 1,400 and 1,500 cm^{-1} (Feldl et al., 2020) correspond to cubic NiO phases with respect to literature.

The Raman spectrum of cubic NiO crystal shows several bands in the investigated region ranging from 450 to 1,800 cm^{-1} [Figure 6(a)]. The bands at ~570 cm^{-1}, ~906 cm^{-1} and ~1,090 cm^{-1} have a vibrational origin and correspond to one-phonon (1P) TO and LO, TO + LO and 2LO modes respectively. It has been reported that the disorder-induced 1P band at ~570 cm^{-1} has very small intensity indicating good quality of single-crystal (Qiu et al., 2022). This confirms that the NiO thin film obtained at pH = 14 for 60 dipping cycles has neither impurities nor secondary phases which agrees with the XRD pattern displayed in Figure 1.

3.5 FTIR analysis

Figure 6(b) shows FTIR spectrum of the prepared NiO thin film deposited at 80 dipping cycles. The bands of the region ranging from 400 to 876 cm^{-1} are due to the bending vibration of the face-centred cubic phase Ni-O (Taşdemirci, 2019). The peaks at 463 cm^{-1}, 668 cm^{-1}, 753 cm^{-1} and 876 cm^{-1} correspond to the nickel-oxide (Ni-O) vibrational modes of the prepared thin films of NiO (Das et al., 2018). The weak peaks around 1,410 cm^{-1} (1,375 and 1,458 cm^{-1}) are related to the residual carbon species present in precursor solution (Das et al., 2018; Taşdemirci, 2019). These appearing at 1,614 cm^{-1}, 2,175 cm^{-1} and 2,360 cm^{-1} respectively are assigned to the bending vibrations of the water molecules (Das et al., 2018).

Figure 6 (a) Raman spectra of NiO thin film deposited at pH = 14 for 60 dipping cycles and annealed at 550°C (b) FTIR image of NiO thin film deposited at pH = 14 for 60 dipping cycles and annealed at 550°C (see online version for colours)

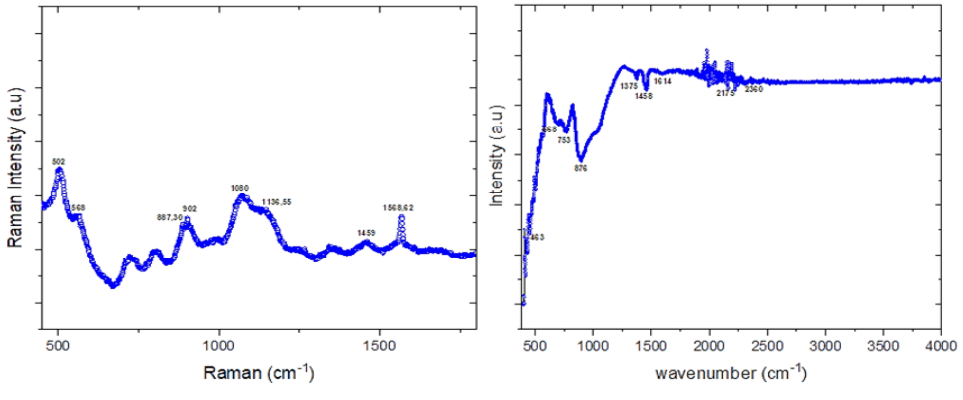

(a) (b)

3.6 SCAPS simulation

3.6.1 Methodology

The optimising of some physical parameters of the HTL, such as its doping concentration, bandgap, electron affinity, defect density, capture cross, and work function … can help reduce the overall series resistance (R_s) of the SC and improve its performance. For this, we have investigated our SC by varying the values of bandgap, electron affinity, mobility of carrier charges and the acceptor doping concentration of NiO HTL, to get the high efficiency possible. That's why we used the SCAPS-1D simulator that is a freely available software package created by the Department of Electronics and Information Systems (ELIS) at Ghent University, Belgium (Burgelman et al., 2004). The work done by SCAPS is based on the resolution of the electrostatic Poisson's equation [equation (4)], the continuity of the electron [equation (5)], and the hole [equation (6)] carriers (Herz, 2017), which allows obtaining the performance parameters.

$$\frac{\partial}{\partial x}\left(\varepsilon(x)\frac{\partial \psi}{\partial x}\right) = -\frac{q}{\varepsilon_0}\left[-n + p - N_A^- + N_D^+ + \frac{1}{q}\rho def(n,\, p)\right] \tag{4}$$

$$-\frac{\partial j_n}{\partial x} + G - U_n(n,\, p) = \frac{\partial n}{\partial t} \tag{5}$$

$$-\frac{\partial j_p}{\partial x} + G - U_p(n,\, p) = \frac{\partial p}{\partial t} \tag{6}$$

where q is the charge of the electron, n and p are the concentration of mobile carrier charge of electrons and holes, respectively, $\rho def(n, p)$ is the defect distribution, ε is the permittivity, Ψ is the electrostatic potential, $U_{p,n}$ is the recombination ratio and G is the generation ratio, j_n and j_p are electron and hole current densities, respectively.

3.6.2 Device simulation and key parameters

Our work is based on a previous work (Bouri et al., 2022), using the same physical parameters to obtain a good approach for our simulation, with FTO/NiO/perovskite/PCBM/BPC/Ag SC structure [Figure 7(a)], the main physical parameters used are collected in Tables 4 and 5 (Bouri et al., 2022; Mushtaq et al., 2023; Mouchou et al., 2021), with the use of our layer parameters NiO.

The layer has good features to use it as HTL. We also used the defect concentration of 10^{14} cm^{-3} for the NiO and the absorption coefficient α which is determined using the following expression [equation (7)] (Bouri et al., 2022):

$$\alpha = A_\alpha \left(hv - E_g\right)^{\frac{1}{2}} \tag{7}$$

where $A\alpha = 102$ is a factor of proportionality and hv is the incident photon energy.

The performance parameters obtained are presented in Table 6, in which JSC is the current of court circuit, V_{oc} is the voltage of open circuit, FF is the fill factor and PCE is the PCE. Figure 8 shows the current-voltage curve of our device which is in a good agreement with other studies (Bouri et al., 2022; Wu et al., 2018).

Table 4 Physical parameters of the SC

Parameters	*NiO_x*	*Perovskite*	*PCBM*
Thickness (nm)	30	250	55
Band gap (E_g) (eV)	3.6	1.6	2
Electron affinity (χ) (eV)	1.8	3.9	3.9
Dielectric permittivity	11.7	28.8	3.9
CB effective density of states (cm^{-3})	2.5×10^{20}	2.2×10^{20}	2.5×10^{21}
VB effective density of states (cm^{-3})	2.5×10^{20}	2.2×10^{20}	2.5×10^{21}
Electron mobility (cm^2/V_s)	10^{-3}	2.2	2×10^{-3}
Hole mobility (cm^2/V_s)	10^{-3}	2.2	2×10^{-4}
Shallow donor density ND (cm^{-3})	0	10^{17}	10^{21}
Shallow acceptor density N_A (cm^{-3})	10^{18}	0	0

Table 5 Defect parameters of the SC

	NiO_x	*Perovskite*	*PCBM*
Defect type	Neutral	Neutral	Neutral
Capture cross section for electron and hole (cm^{-2})	10^{-15}	10^{-15}	10^{-15}
Energetic distribution	Single	Single	Single
Energy level with respect to E_v	0.6	0.6	0.6
Total density (cm^{-3})	10^{14}	2.67×10^{15}	10^{10}

Figure 7 (a) SC structure (b) Flat band energy diagram (see online version for colours)

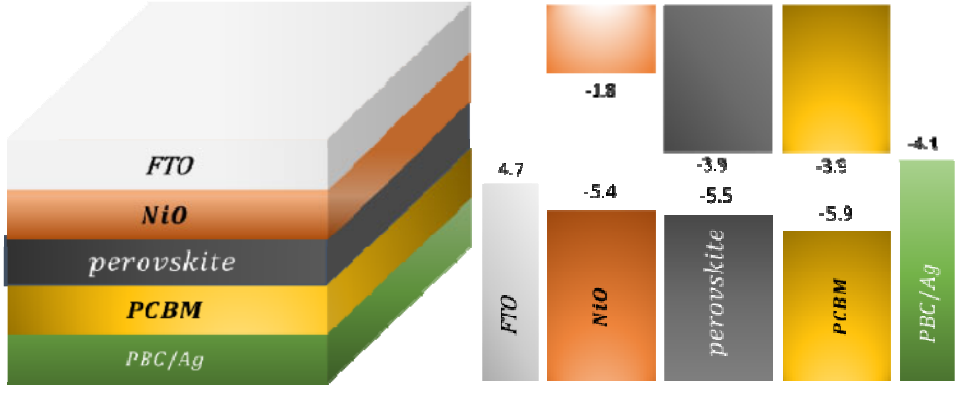

(a) (b)

Table 6 Performance parameters comparison, our work versus literature

	V_{oc} (V)	*J_{sc} (mA/cm^2)*	*FF (%)*	*PCE (%)*
This work	1.02	20.53	75.22	15.75
Literature	1.02	20.80	74.20	15.70

Figure 8 Current-voltage curve (see online version for colours)

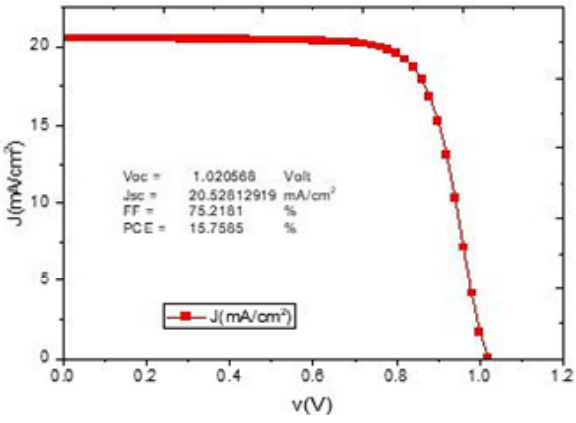

3.6.3 Effect of band gap and electron affinity of the HTL on SC performances

The performance of the SC is affected significantly, by the type of the HTL, which can enhance the positive carrier charges transport and extraction from the active layer (perovskite) (Yao et al., 2022). This is a result of the alignment of the band energy between both HTL and active layer [Figure 7(b)], and that's also controlled by the electron affinity. The configuration of the values of bandgap and the electron affinity simultaneously, is very important to achieve a high PCE and improve the other performance parameters. Figure 9 presents the performance parameters resulting from the variation of the bandgap and the electron affinity respectively from 3.0 eV to 3.8 eV and from 1.63 eV to 2 eV, at the same time.

The J_{sc} took the lowest values between the bandgap values of 3.7 eV and 3.8 eV, as well as the values of the electron affinity range of 1.96 eV and 2 eV, on the other side took the values higher than 20.24 mA.cm^{-2} [Figure 9(c)]. Voc shows almost all high values below the 1.026 V contour and low values for all higher values. Thus, the higher V_{oc} is according to the net values between 3.0 eV–3.4 eV for the bandgap variable and 1.67 eV–2.0 eV for the electron affinity variable [Figure 9(b)].

The PCE and the FF show the same variation, where the maximum values are in the middle of the curve delimited by the contours 75.73% for FF and 15.93% for PCE, respectively the higher are 84.3% and 18.1% (Figures 9(a) and 9(d)], correspond to the configuration of the values of the band gap and electron affinity parameters given in Table 7. Figure 10 illustrates that the alignment energy band has been affected by the variation of both E_g and χ following the formula [equation (8)] in which the vacuum energy is E_{vac} and the valance energy is E_v (Cendula et al., 2014; Kahn, 2016). As a result, the difference between all performance parameters was found.

$$E_{vac} = E_v + E_g + \chi \tag{8}$$

Figure 9 Effect of band gap and electron affinity values combination on the performance parameters of SC (see online version for colours)

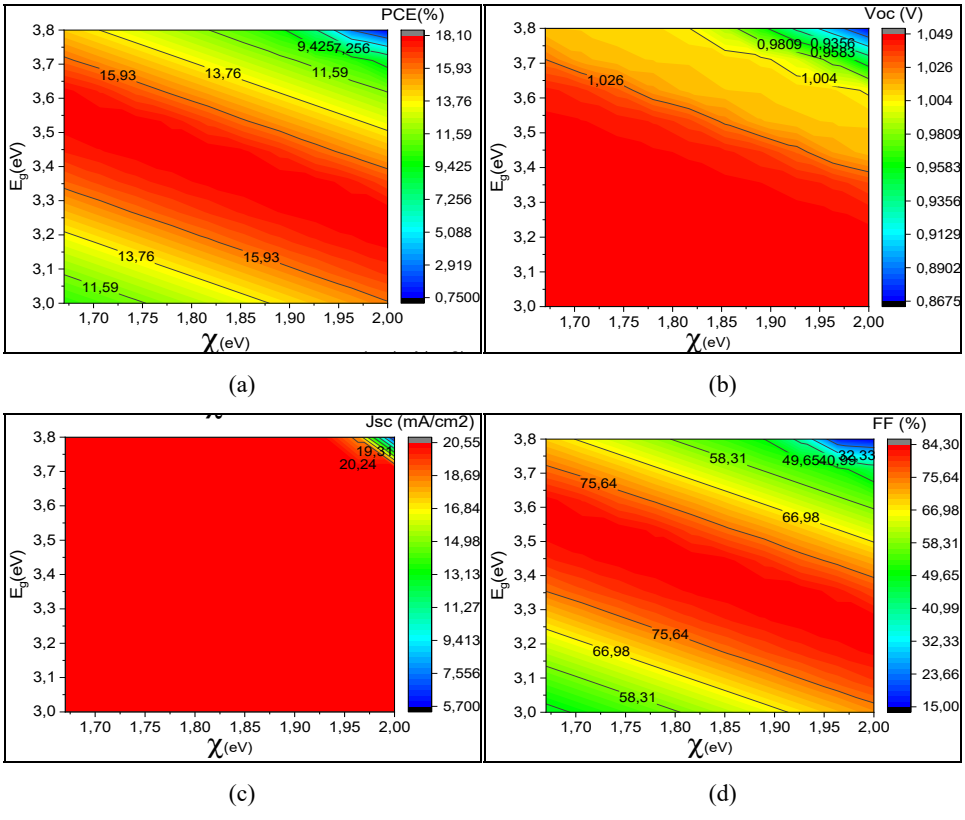

Figure 10 SC diagram band energy variation for same combination values of band gap and electron affinity (see online version for colours)

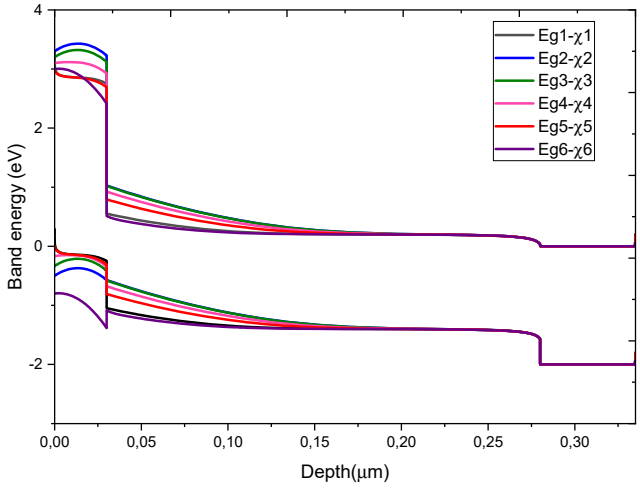

Table 7 Combination of band gap and electron affinity values gave the highest PCE

Electron affinity (eV)	1.89	1.71	1.96	1.78	1.82
Band gap (eV)	3.36	3.53	3.27	3.44	3.44
FF (%)	84.3	84.3	84.3	84.3	84.3
PCE (%)	18.1	18.1	18.1	18.1	18.1

3.6.4 Effect of the HTL carrier charges mobility on SC performances

The mobility of carrier charges is a crucial physical parameter that influences the overall performance of SCs. High HTL hole mobility is desirable in a SC because it allows the holes to move more freely, reducing the probability of recombination and device resistance, and improving charge extraction and collection (Wang et al., 2022). The range of variation in hole and electron mobility is between 0.001 cm^2/V_s and 2.8 cm^2/V_s, which is verified simultaneously. The results are shown in Figure 11. The variation in electron mobility did not affect the performance parameters to any great or significant extent. Furthermore, the variation in hole mobility influences mainly the FF, which imposes its variation on the PCE [Figures 11(a) and 11(d)]. The highest values of J_{sc} = 20.53 mA/cm^2, V_{oc} = 1.02 V, FF = 81.40% and PCE = 17.06% are obtained between 1.4 cm^{-2}/V_s and 2.8 cm^{-2}/V_s for the hole and for all electron mobility values [Figures 11(a), 11(b), 11(c) and 11(d)]. This variation is due to the series resistance being reduced by the increase in the hole mobility from 6.07 Ωcm^2 to 0.69 Ωcm^2, in which the PCE is improved. Table 8 summarises the initial and optimised parameters and results.

Table 8 Combination of hole and electron mobility values gave the highest PCE

	μ_p	μ_n	R_s (Ωcm^2)	PCE (%)	J_{sc} (mA/cm^{-2})	V_{oc} (V)	FF (%)
Initial	0.001	0.001	6.07	15.76	20.53	1.02	75.22
Optimisation	2.8	0.001	0.69	17.06	20.53	1.02	81.40

3.6.5 Effect of the HTL acceptor concentration (N_A) on SC performances

To study the effect of acceptor carrier charge concentration on our simulated SC we varied the by taking the values between 10^{15} cm^{-3} and 10^{18} cm^{-3}. Figure 12 shows the N_A impact of NiO HTL on the performance parameters. V_{oc} slightly decreases with the N_A increase of N_A. J_{sc} also shows a slight increase. The FF increases from 64.47% at $N_A = 10^{15}$ cm^{-3} to a value of 75.23% for $N_A = 10^{18}$ cm^{-3}. This change in FF, as a parameter that measured the film quality, is due to the decrease in the R_s of the SC, from 11.42 Ωcm^2 at $N_A = 10^{15}$ cm^{-3} to 6.07 Ωcm^2 at $N_A = 10^{18}$ cm^{-3}. The curves show that the FF is the main performance parameter that influenced the PCE. This also due to the higher current flow through the cell created with the increase in N_A, which increases conductivity and enhance PCE (Bouazizi et al., 2022).

The PCE shows almost the same variation mode of FF, which increases from 13.73% at $N_A = 10^{15}$ cm^{-3} to the value of 15.76% at $N_A = 10^{18}$ cm^{-3}. Table 9 summarises the values of performance parameters and series resistance for both values of $N_A = 10^{15}$ cm^{-3} and $N_A = 10^{18}$ cm^{-3}, showing its effect. Hence, the optimum value of N_A is 10^{18} cm^{-3} that is in good agreement with numerous works (Ahmmed et al., 2020; Raza et al., 2021).

Figure 11 Effect of hole and electron values combination on the performance parameters of SC (see online version for colours)

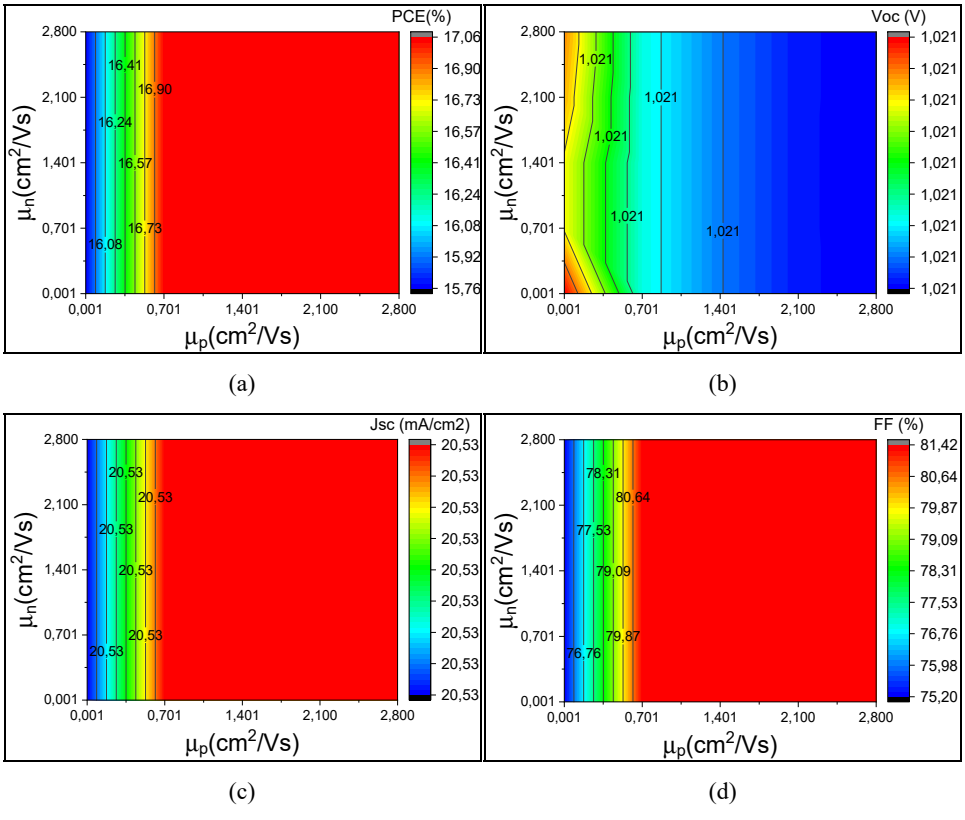

Table 9 The difference between the R_s and the performance parameters given by low $N_A = 10^{15}$ and high $N_A = 10^{18}$ values

N_A	R_s (Ωcm^2)	PCE (%)	J_{sc} (mA/cm^{-2})	V_{oc} (V)	FF (%)
10^{15}	11.42	13.73	20.38	1.05	64.47
10^{18}	6.06	15.76	20.53	1.02	75.23

3.6.6 Optimum physical parameters and results

In this last part of the simulation, we collected all the optimal key parameters obtained: 3.44 eV, χ = 1.82 eV, μ_p = 2.8 cm^2/V_s and μ_n = 0.001 cm^2/V_s using them to reach the highest possible PCE, the results of which are shown in the Table 10.

Table 10 Comparison between initial and optimised performance parameters

	PCE (%)	J_{sc} (mA/cm^{-2})	V_{oc} (V)	FF (%)
Optimisation	18.11	20.52	1.05	84.46

From the SCAPS simulation, the optimal band gap of 3.44 eV with PCE of 18.11% agrees with the experimental study in which the NiO thin film was successfully grown at pH = 14 for 60 cycles and annealed at 550°C for two hours. The thin film is suitable as HTL for the PSC with a PCE of 18.11%.

Figure 12 Effect of N_A on the performance parameters of SC

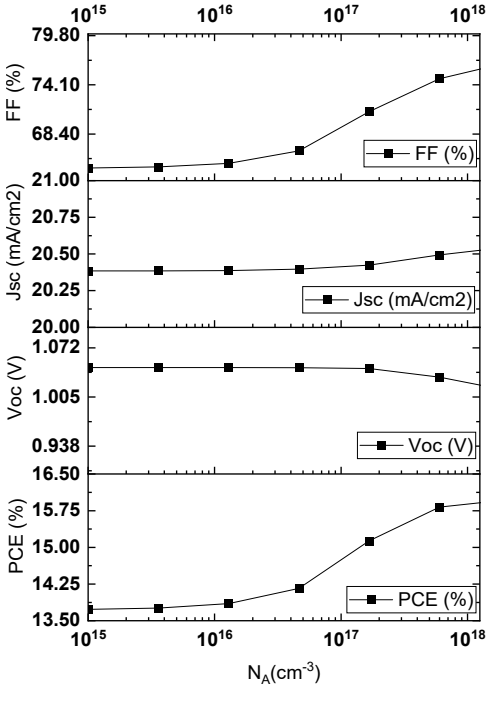

4 Conclusions

In the present work, an adherent and well crystallised NiO thin film was successfully grown by SILAR technique at pH = 14 and for tree dipping cycles 20, 60 and 80. Which the optical bands gap was extracted from the Tauc plot, that given respectively 3.27 eV, 3.44 eV and 3.18 eV. The transmittance of the film was 86%. The pure cubic NiO phase with the diffraction planes (111), (200) and (220) was confirmed by Raman spectroscopy thanks to the disorder-induced 1P band at ~570 cm^{-1} with a very small intensity indicating good quality of single-crystal. The peaks at 463 cm^{-1}, 668 cm^{-1}, 753 cm^{-1} and 876 cm^{-1} correspond to the nickel-oxide (Ni-O) vibrational modes of the prepared thin films of NiO based on FTIR analysis. After that SCAPS simulation was carried out to optimise the band gap for a better PCE of the PSC.

The optimal band gap of the simulation study agreed with the experimental one which is 3.44 eV with a PCE of 18.11%. The NiO thin film can be used as an HTL for the PSC which is a promising result that must be improved in perspectives.

References

Ade, R., Ganesh, V., Bitla, Y. and Kumar, Y.V. (2022) 'Optoelectronic properties of spray pyrolyzed NiO: Pr thin films', *Applied Physics A*, Vol. 128, p.517, https://doi.org/10.1007/s00339-022-05636-4.

Aftab, M., Butt, M.Z., Ali, D., Bashir, F. and Khan, T.M. (2021) 'Optical and electrical properties of NiO and Cu-doped NiO thin films synthesized by spray pyrolysis', *Optical Materials*, Vol. 119, p.111369, https://doi.org/10.1016/j.optmat.2021.111369.

Ahmmed, S., Aktar, A., Rahman, M.F., Hossain, J. and Ismail, A.B.M. (2020) 'A numerical simulation of high efficiency CdS/CdTe based solar cell using NiO HTL and ZnO TCO', *Optik*, Vol. 223, p.165625, https://doi.org/10.1016/j.ijleo.2020.165625.

Ai, L., Fang, G., Yuan, L., Liu, N., Wang, M., Li, C., Zhang, Q., Li, J. and Zhao, X. (2008) 'Influence of substrate temperature on electrical and optical properties of p-type semitransparent conductive nickel oxide thin films deposited by radio frequency sputtering', *Appl. Surf. Sci*., Vol. 254, pp.2401–2405, https://doi.org/10.1016/j.apsusc.2007.09.051.

Aivalioti, C., Manidakis, E.G., Pelekanos, N.T., Androulidaki, M., Tsagaraki, K., Viskadourakis, Z. et al. (2023) 'Niobium-doped NiO as p-type nanostructured layer for transparent photovoltaics', *Thin Solid Films*, Vol. 778, p.139910, https://doi.org/10.1016/j.tsf.2023.139910.

Akaltun, Y. and Çayır, T. (2015)"Fabrication and characterization of NiO thin films prepared by SILAR method', *Journal of Alloys and Compounds*, Vol. 625, pp.144–148, https://doi.org/10.1016/j.jallcom.2014.10.194.

Aswathy, N.R., Varghese, J. and Vinod Kumar, R. (2022) 'Photocatalytic degradation of malachite green using vanadium pentoxide-doped NiO thin film by sol-gel spin coating', *The European Physical Journal Plus*, Vol. 137, p.1344, https://doi.org/10.1140/epjp/s13360-022-03559-w.

Aswathy, N.R., Varghese, J. and Vinodkumar, R. (2020) 'Effect of annealing temperature on the structural, optical, magnetic and electrochemical properties of NiO thin films prepared by sol-gel spin coating', *Journal of Materials Science: Materials in Electronics*, Vol. 31, pp.16634–16648, https://doi.org/10.1007/s10854-020-04218-5.

Bahramian, A., Eyraud, M., Vacandio, F., Hornebecq, V., Djenizian, T. and Knauth, P. (2019) 'Single-step electrodeposition of superhydrophobic black NiO thin films', *Journal of Applied Electrochemistry*, Vol. 49, pp.621–629, https://doi.org/10.1007/s10800-019-01305-2.

Bouazizi, S., Tlili, W., Bouich, A., Soucase, B.M. and Omri, A. (2022) 'Design and efficiency enhancement of FTO/PC 60 BM/CsSn 0.5 Ge 0.5 I 3/spiro-OMeTAD/Au perovskite solar cell utilizing SCAPS-1D simulator', *Mater. Res. Express*, Vol. 9, No. 9, DOI: 10.1088/2053-1591/ac8d52.

Bouri, N., Talbi, A., Khaaissa, Y., Derbali, S., Bouich, A. and Nouneh, K. (2022) 'Insight into MA Pb 1 – x Eu x I 3 based perovskite solar cell performance using SCAPS simulator', *Optik*, Vol. 271, p.170235, https://doi.org/10.1016/j.ijleo.2022.170235.

Bulakhe, S.C. and Deokate, R.J. (2022) 'Electrochemically prepared Fe: NiO thin film catalysis for oxygen evolution reaction', *Journal of Materials Science: Materials in Electronics*, Vol. 33, pp.18180–18186, https://doi.org/10.1007/s10854-022-08674-z.

Burgelman, M., Verschraegen, J., Degrave, S. and Nollet, P. (2004) 'Modeling thin-film PV devices', *Prog. Photovolt.: Res. Appl.*, Vol. 12, pp.143–153, https://doi.org/10.1002/pip.524.

Cai, X., Hu, T., Hou, H., Zhu, P., Liu, R., Peng, J. et al. (2023) 'A review for nickel oxide hole transport layer and its application in halide perovskite solar cells', *Materials Today Sustainability*, Vol. 23, p.100438, https://doi.org/10.1016/j.mtsust.2023.100438.

Calixto-Rodriguez, M., Valdez Martínez, J.S., Meneses-Arcos, M.A., Ortega-Cruz, J., Sarmiento-Bustos, E., Reyes-Mayer, A. et al. (2021) 'Design and development of software for the SILAR control process using a low-cost embedded system', *Processes*, Vol. 9, No. 6, p.967, https://doi.org/10.3390/pr9060967.

Cendula, P., Tilley, S.D., Gimenez, S., Bisquert, J., Schmid, M., Grätzel, M. and Schumacher, J.O. (2014) 'Calculation of the energy band diagram of a photoelectrochemical water splitting cell', *J. Phys. Chem. C*, Vol. 118, No. 51, pp.29599–29607.

Chtouki, T., El Mrabet, M., Tarbi, A., Goncharova, I. and Erguig, H. (2021) 'Comprehensive review of the morphological, linear and nonlinear optical characterization of spin-coated NiO thin films for optoelectronic applications', *Optical Materials*, Vol. 118, p.111294, DOI: 10.1016/j.optmat.2021.111294.

Das, M.R., Roy, A., Mpelane, S., Mukherjee, A., Mitra, P. and Das, S. (2018) 'Influence of dipping cycle on SILAR synthesized NiO thin film for improved electrochemical performance', *Electrochimica Acta*, Vol. 273, pp.105–114.

Dridi, W., Jouini, K., Daoudi, M., Hosni, F. and Bignan, G. (2023) 'Neutron reactor dosimetry monitoring by optical, nanostructural, and morphological changes of NiO thin films', *Radiation Physics and Chemistry*, Vol. 203, Part A, p.110639, https://doi.org/10.1016/j.radphyschem.2022.110639.

Fasaki, I., Koutoulaki, A., Kompitsas, M. and Charitidis, C. (2010) 'Structural, electrical and mechanical properties of NiO thin films grown by pulsed laser deposition', *Applied Surface Science*, Vol. 257, No. 2, pp.429–433, https://doi.org/10.1016/j.apsusc.2010.07.006.

Feldl, J., Budde, M., Tschammer, C., Bierwagen, O. and Ramsteiner, M. (2020) 'Magnetic characteristics of epitaxial NiO films studied by Raman spectroscopy', *Journal of Applied Physics*, Vol. 127, p.235105, https://doi.org/10.1063/5.0006085.

Ganesh, V., Kumar, B.R., Bitla, Y., Yahia, I.S. and AlFaify, S. (2021) 'Structural, optical and dielectric properties of Nd doped NiO thin films deposited with a spray pyrolysis method', *Journal of Inorganic and Organometallic Polymers and Materials*, Vol. 31, pp.2691–2699, https://doi.org/10.1007/s10904-021-01889-3.

Ganga Reddy, K., Nagaraju, P., Reddy, G.L.N., Ghosal, P. and Reddy, M.V.R. (2022) 'Growth and characterization of electron beam evaporated NiO thin films for room temperature formaldehyde sensing', *Sensors and Actuators A: Physical*, Vol. 346, p.113876, https://doi.org/10.1016/j.sna.2022.113876.

Goel, R., Jha, R., Bhushan, M., Bhardwaj, R. and Ravikant, C. (2022) 'Hydrothermally synthesized nickel oxide (NiO) nano petals', *Materials Today: Proceedings*, Vol. 48, pp.687–689.

Gutierrez, A., Perpiñán, M.F., Sánchez, A.E. and Torralba, M.C. (2013) 'Solvotermal synthesis of NiO, Ni and NiS nanoparticles', *Journal of Nanoscience and Nanotechnology*, January, Vol. 13, No. 1, pp.461–466, DOI: 10.1166/jnn.2013.6717. PMID: 23646755.

Herz, L.M. (2017) 'Charge-carrier mobilities in metal halide perovskites: fundamental mechanisms and limits', *ACS Energy Letters*, Vol. 2, No. 7, p.1539, DOI: 10.1021/acsenergylett.7b00276.

Hosseinzade, M.R., Naji, L. and Hasannezhad, F. (2022) 'Electrochemical deposition of NiO bunsenite nanostructures with different morphologies as the hole transport layer in polymer solar cells', *Journal of Electroanalytical Chemistry*, Vol. 926, p.116955, https://doi.org/10.1016/j.jelechem.2022.116955.

Javadian, A. and Fadavieslam, M.R. (2022) 'Impact of copper doping in NiO thin films deposited by spray pyrolysis on their physical properties', *Journal of Materials Science: Materials in Electronics*, Vol. 33, pp.23362–23374, https://doi.org/10.1007/s10854-022-09098-5.

Jiang, D.Y., Qin, J.M., Wang, X., Gao, S., Liang, Q.C. and Zhao, J.X. (2012) 'Optical properties of NiO thin films fabricated by electron beam evaporation', *Vacuum*, Vol. 86, No. 8, pp.1083–1086, https://doi.org/10.1016/j.vacuum.2011.10.003.

Jlassi, M., Sta, I., Hajji, M. and Ezzaouia, H. (2017) 'NiO thin films synthesized by sol-gel: potentiality for the realization of antireflection layer for silicon based solar cell applications', *Surfaces and Interfaces*, Vol. 6, pp.218–222, https://doi.org/10.1016/j.surfin.2016.10.006.

Kahn, A. (2016) 'Fermi level, work function and vacuum level', *Mater. Horiz.*, Vol. 3, p.7, DOI: https://doi.org/10.1039/C5MH00160A.

Kaya, D., Aydınoğlu, H.S., Tüzemen, E.Ş. and Ekicibil, A. (2021) 'Investigation of optical, electronic, and magnetic properties of p-type NiO thin film on different substrates', *Thin Solid Films*, Vol. 732, p.138800, https://doi.org/10.1016/j.tsf.2021.138800.

Klochko, N.P., Klepikova, K.S., Zhadan, D.O., Petrushenko, S.I., Kopach, V.R., Khrypunov, G.S. et al. (2018) 'Structure, optical, electrical and thermoelectric properties of solution-processed Li-doped NiO films grown by SILAR', *Materials Science in Semiconductor Processing*, Vol. 83, pp.42–49, https://doi.org/10.1016/j.mssp.2018.04.010.

Mattaparthi, S., Sinha, D.K., Bhura, A. and Khosla, R. (2023) 'Design of an eco-friendly perovskite Au/NiO/FASnI3/ZnO0.25S0.75/FTO, device structure for solar cell applications using SCAPS-1D', *Results in Optics*, Vol. 12, p.100444, https://doi.org/10.1016/j.rio.2023.100444.

Mironova-Ulmane, N., Kuzmin, A., Steins, I., Grabis, J., Sildos, I. and Pärs, M. (2007) 'Raman scattering in nanosized nickel oxide NiO', *Journal of Physics: Conference Series*, Vol. 93, p.12039.

Mouchou, R.T., Jen, T.C., Laseinde, O.T. and Ukoba, K.O. (2021) 'Numerical simulation and optimization of p-NiO/n-TiO_2 solar cell system using SCAPS', *Materials Today: Proceedings*, Vol. 38, p.835.

Mushtaq, S., Tahir, S., Ashfaq, A., Sebastian Bonilla, R., Haneef, M., Saeed, R., Ahmad, W. and Amin, N. (2023) 'Performance optimization of lead-free $MASnBr_3$ based perovskite solar cells by SCAPS-1D device simulation', *Solar Energy*, Vol. 249, p.401, https://doi.org/10.1016/j.solener.2022.11.050.

Nachammai, J., Perumal, P., Deivamani, D. and Saravanakumar, S. (2022) 'Effect of concentrations and characterization of nickel oxide thin films prepared by SILAR method', *Materials Today: Proceedings*, Vol. 64, pp.1789–1792.

Obaida, M., Fathi, A.M., Moussa, I. and Afify, H.H. (2022) 'Characterization and electrochromic properties of NiO thin films prepared using a green aqueous solution by pulsed spray pyrolysis technique', *Journal of Materials Research*, Vol. 37, pp.2282–2292, https://doi.org/10.1557/s43578-022-00627-w.

Owoeye, V.A., Adewinbi, S.A., Salau, A.O., Orelusi, A.N., Adeoye, A.E. and Akindadelo, A.T. (2023) 'Effect of precursor concentration on stoichiometry and optical properties of spray pyrolyzed nanostructured NiO thin films', *Heliyon*, Vol. 9, No. 1, p.e13023, https://doi.org/10.1016/j.heliyon.2023.e13023.

Qin, Y., Song, J., Qiu, Q., Liu, Y., Zhao, Y., Zhu, L. et al. (2019) 'High-quality NiO thin film by low-temperature spray combustion method for perovskite solar cells', *Journal of Alloys and Compounds*, Vol. 810, p.151970, https://doi.org/10.1016/j.jallcom.2019.151970..

Qiu, J., Nguyen, T.H., Kim, S., Lee, Y.J., Song, M-T., Huang, W-J. et al. (2022) 'Two-dimensional correlation spectroscopy analysis of Raman spectra of NiO nanoparticles', *Spectrochimica Acta Part A: Molecular and Biomolecular Spectroscopy*, 5 November, Vol. 280, p.121498, DOI: 10.1016/j.saa.2022.121498. Epub 2022 Jun 13. PMID: 35724591.

Qiu, J., Nguyen, T.H., Lee, Y.J., Kim, S., Kim, S., Kim, S-J. et al. (2023) 'Strong oxygen-content dependence of the magnetic excitations in antiferromagnetic NiO nanoparticles: a Raman probe', *Spectrochimica Acta Part A: Molecular and Biomolecular Spectroscopy*, Vol. 297, p.122700, https://doi.org/10.1016/j.saa.2023.122700.

Quispe, L.T., Avila, L.B., Linhares, A.A., López, E.O., Mello, A., Brandt, I.S. et al. (2021) 'p-type NiO thin films obtained via an electrochemical-thermal route', *Journal of Materials Science: Materials in Electronics*, Vol. 32, pp.5372–5380, https://doi.org/10.1007/s10854-021-05260-7.

Raza, E., Ahmad, Z., Aziz, F., Asif, M., Ahmed, A., Riaz, K., Bhadra, J. and Al-Thani, N.J. (2021) 'Numerical simulation analysis towards the effect of charge transport layers electrical properties on cesium based ternary cation perovskite solar cells performance', *Solar Energy*, Vol. 225, p.842, https://doi.org/10.1016/j.solener.2021.08.008.

Şenaslan, F., Taşdemir, M. and Çelik, A. (2021) 'Effect of working pressure and post-annealing on structural, optical and electrical properties of p-type NiO thin films produced by RF magnetron sputtering technique', *Applied Physics A*, Vol. 127, pp.1–9.

Soonmin, H. (2022) 'Recent advances in the growth and characterizations of SILAR-deposited thin films', *Applied Sciences*, Vol. 12, p.8184, https://doi.org/10.3390/app12168184.

Srivastava, S., Gangwar, A.K., Kumar, A., Gupta, G. and Singh, P. (2023) 'Room temperature RF magnetron sputtered nanocrystalline NiO thin films for highly responsive and selective H2S gas sensing at low PPM concentrations', *Materials Research Bulletin*, Vol. 165, p.112330, https://doi.org/10.1016/j.materresbull.2023.112330.

Sundhar, A. (2022) 'Development of ZnS thin film with Co, Cu and Ag doping using SILAR method', *Materials Today: Proceedings*, Vol. 48, pp.377–381.

Tang, Y., Shen, H., Wang, T., Peng, S., Jin, K., Qian, Q. et al. (2023) 'Study on electrochemical ion behavior and electrochromic properties of NiO thin films prepared by magnetron sputtering with different oxygen levels', *Thin Solid Films*, Vol. 769, p.139754, https://doi.org/10.1016/j.tsf.2023.139754.

Taşdemirci, T.Ç. (2019) 'Influence of annealing on properties of SILAR deposited nickel oxide films', *Vacuum*, Vol. 167, pp.189–194, https://doi.org/10.1016/j.vacuum.2019.05.047.

Terlemezoglu, M., Surucu, O., Isik, M., Gasanly, N.M. and Parlak, M. (2022) 'Temperature-dependent optical characteristics of sputtered NiO thin films', *Applied Physics A*, Vol. 128, pp.1–6, DOI: 10.1007/s00339-021-05197-y.

Usha, K.S., Sivakumar, R. and Sanjeeviraja, C. (2022) 'Preparation of pure NiO thin film by radio frequency magnetron sputtering technique and investigation on its properties', *Journal of Materials Science: Materials in Electronics*, Vol. 33, pp.16136–16143, https://doi.org/10.1007/s10854-022-08504-2.

Vijaya Prasath, G., Usha, K.S., Karuppaiah, M., Ravi, G. and Krishnan, P. (2022) 'Fabrication of heterostructure NiO/ZnO thin film for pseudocapacitor application', *Journal of Sol-Gel Science and Technology*, Vol. 104, pp.198–210, https://doi.org/10.1007/s10971-022-05919-5.

Wang, R. et al. (2022) 'High-hole-mobility metal-organic framework as dopant-free hole transport layer for perovskite solar cells', *Nanoscale Res. Lett*., Vol. 17, p.6, https://doi.org/10.1186/s11671-021-03643-7.

Woo-García, R.M., Rodríguez-Ibarra, I., Osorio-de-la-Rosa, E., Guarneros-Aguilar, C., Caballero-Briones, F., Agustín-Serrano, R. et al. (2022) 'Automated instrument for the deposition of thin films using successive ionic layer adsorption and reaction', *Processes*, Vol. 10, p.492, https://doi.org/10.3390/pr10030492.

Wu, X., Li, H., Wang, K., Sun, X. and Wang, L. (2018) "CH3NH3 Pb 1 – x Eu x I 3 mixed halide perovskite for hybrid solar cells: the impact of divalent europium doping on efficiency and stability', *RSC Advances*, Vol. 8, No. 20, pp.11095–11101, https://doi.org/10.1039/c7ra12754e.

Xiao, D., Li, X., Wang, D., Li, Q., Shen, K. and Wang, D. (2017) 'CdTe thin film solar cell with NiO as a back contact buffer layer', *Solar Energy Materials and Solar Cells*, Vol. 169, pp.61–67, https://doi.org/10.1016/j.solmat.2017.05.006.

Yao, Y., Cheng, C., Zhang, C., Hu, H., Wang, K. and De Wolf, S. (2022) 'Organic hole-transport layers for efficient, stable, and scalable inverted perovskite solar cells', *Advanced materials (Deerfield Beach, Fla.)*, Vol. 34, No. 44, p.e2203794, https://doi.org/10.1002/adma.202203794.

Youn, S-M., Park, M-J., Kim, J.H. and Jeong, C. (2020) 'Performance enhancement of CIGS thin-film solar cells with a functional-window NiO thin layer', *Journal of Alloys and Compounds*, Vol. 836, p.154803, https://doi.org/10.1016/j.jallcom.2020.154803.

Zhao, X., Liang, Y., Xue, L., Li, G. and Guo, F. (2022) 'Numerical simulation and performance optimization of GeSe based thin film solar cell with NiO as back surface field layer', *Optical Materials*, Vol. 131, p.112707, https://doi.org/10.1016/j.optmat.2022.112707.

Nomenclatures

XRD	X-ray diffraction
SEM	Scanning electron microscopy
EDX	Energy dispersive X-ray spectroscopy
HTL	Hole transport layer
PSC	Perovskite solar cell
SC	Solar cell
PCE	Power conversion efficiency
FF	Fill factor